Neurosurg Rev (2014) 37:481–492
DOI 10.1007/s10143-014-0550-x

ORIGINAL ARTICLE

Brainstem cavernoma surgery with the support of pre- and postoperative diffusion tensor imaging: initial experiences and clinical course of 23 patients

Nils H. Ulrich · Ralf A. Kockro · David Bellut · Christina Amaxopoulou · Oliver Bozinov · Jan-Karl Burkhardt · Johannes Sarnthein · Spyros S. Kollias · Helmut Bertalanffy

Received: 14 April 2013 / Revised: 20 August 2013 / Accepted: 19 January 2014 / Published online: 7 May 2014

Abstract The spatial complexity of highly vulnerable structures makes surgical resection of brainstem cavernomas (BSC) a challenging procedure. Diffusion tensor imaging (DTI) allows for the visualization of white matter tracts and enables a better understanding of the anatomical location of corticospinal and sensory tracts before and after surgery.We investigated the feasibility and clinical usefulness of DTI-based fiber tractography in patients with BSC.Pre- and postoperative DTI visualization of corticospinal and sensory tracts were retrospectively analyzed in 23 individuals with BSC. Preoperative and postoperative DTI-fiber accuracy were associated to the neurological findings. Preoperatively, the corticospinal tracts were visualized in 90 % of the cases and the sensory tracts were visualized in 74 % of the cases. Postoperatively, the corticospinal tracts were visualized in 97 % of the cases and the sensory tracts could be visualized in 80 % of the cases. In all cases, the BSC had caused displacement, thinning, or interruption of the fiber tracts to various degrees. Tract visualization was associated with pre- and postoperative neurological findings. Postoperative damage of the corticospinal tracts was observed in two patients. On follow-up, the Patzold Rating (PR) improved in 19 out of 23 patients (83 %, p= 0.0002).This study confirms that DTI tractography allows accurate and detailed white matter tract visualization in the brainstem, even when an intraaxial lesion affects this structure. Furthermore, visualizing the tracts adjacent to the lesion adds to our understanding of the distorted intrinsic brainstem anatomy and it may assists in planning the surgical approach in specific cases.

Keywords Diffusion tensor imaging · Magnetic resonance imaging · Brainstem tumor · Surgical planning · Brainstem cavernoma · Neurological rating of Patzold · Brainstem anatomy

Nils H. Ulrich and Ralf A. Kockro contributed equally to this work.

Electronic supplementary material The online version of this article (doi:10.1007/s10143-014-0550-x) contains supplementary material, which is available to authorized users.

N. H. Ulrich (✉) · D. Bellut · O. Bozinov · J.-K. Burkhardt · J. Sarnthein
Department of Neurosurgery, University Hospital, University of Zurich, Frauenklinikstr.10, 8091 Zurich, Switzerland
e-mail: nils.hb.ulrich@gmail.com

R. A. Kockro
Department of Neurosurgery, Hirslanden Hospital, Zurich, Switzerland

C. Amaxopoulou · S. S. Kollias
Department of Neuroradiology, University Hospital, University of Zurich, Zurich, Switzerland

H. Bertalanffy
International Neuroscience Institute, INI, Hannover, Germany

Introduction

Surgical resection of brainstem cavernomas (BSC) remains a major challenge for the neurosurgeon and the operating team. With improvements in neuroimaging and microsurgical techniques, surgical indications for BSC could be extended. The management of these lesions is based on clinical and radiological findings and largely depends on surgical experience [5–7, 12, 22, 29, 32, 37].

Increasingly detailed anatomical knowledge gained from fiber dissections has been crucial for the understanding of white matter paths [35]. On that basis, it appears to be of great benefit to determine the association between the lesion and the eloquent white matter tracts in order to establish the best neurosurgical approach. In the late 1990s, magnetic resonance imaging techniques allowed for the visualization of

anisotropic diffusion tensor maps, as well as the calculation and three-dimensional display of resulting white matter tracts. This technique has proven to provide anatomical-structural information [2, 3, 11, 24] to improve the surgical management of gliomas [9, 15, 27, 38] and arteriovenous malformations (AVM) [17], and it is also used in the fields of functional neurosurgery [4, 31] and radiosurgery [19]. In the region of the brainstem that represents a special visualization challenge due to its densely packed anatomic structures, diffusion tensor imaging has been successfully used in the surgical planning process for gliomas and cavernomas. Moreover, several groups have shown that diffusion tensor imaging (DTI)-based tractography allows for the depiction of white matter tracts, even in the densely packed region of the brainstem [8, 9, 15, 18, 27].

In our institution, we have been using DTI tractography on a regular basis for the preoperative visualization and surgical planning in patients that harbor lesions in eloquent supra- and infratentorial regions, including the BSC. Here, we present our experiences with 23 BSC patients who were analyzed by DT-imaging to visualize the corticospinal and sensory tracts with regard to surgical considerations and patient outcome.

Patients and methods

Patient characteristics

This retrospective single-center study included 23 patients (5 men, 18 women) with a mean age of 36 years (±15; 6 to 63 years). Each of them underwent microsurgical resection of a symptomatic BSC at the Department of Neurosurgery, University Hospital Zurich, Switzerland. The study was approved by the independent Ethics Committee of the Kanton Zurich (Projekt E-55/2008). All surgeries were performed by the senior author (H.B.) between 2008 and 2010 in accordance with the institutional guidelines and after the patients' written consent. On behalf of minors/children participants involved in our study, we obtained written consent by their legal guardians.

In seventeen patients, the cavernoma was located in the pons (74 %), 3 lesions were within the midbrain (13 %), one lesion was in the medulla (4 %), one was in the crus cerebri (4 %), and one was in the cerebellar peduncle (4 %) (Table 1).

Clinical assessment and neurological status

Patient data, including clinical and neurological status, were retrospectively obtained upon admission and upon discharge with a special focus on sensory-motor deficits. Motor strength was graded from strength level 0 (complete plegia) to level 5 (full strength) by using the Medical Research Council Scale of 0–5 [14]. Sensory disturbances were graded either absent, mild, or severe (Table 1: absent 1, mild 2, severe 3).

The neurological status of all patients at the preoperative period, upon discharge and upon follow-up was classified using the Karnofsky Performance Status Scale (KPS). KPS scores range from 0 (dead) to 100 (no evidence of disease). Furthermore, we used the Patzold Rating (PR) to perform a broader classification [13]. The rating was employed upon admission, discharge, and once again upon follow-up. All clinical information was retrospectively derived from official admission reports, clinical notes, and discharge letters. Histopathological analysis of the resected lesions revealed the presence of BSCs in all 23 patients.

Conventional MR imaging and diffusion tensor imaging

All radiological images were provided and analyzed by the Department of Neuroradiology, University of Zurich, Switzerland. T1- and T2-weighted MRI images, as well as DTI studies, were obtained as part of a pre- and postoperative routine at this institution. A senior board-certified neuroradiologist, blinded to the clinical characteristics and outcome of the patients, performed the analysis.

Conventional MRI data acquisition

A 3 T whole body MR system (Philips Achieva, Best, Netherlands), equipped with 80 mT/m/ms gradient coils and an 8-element receive head coil array (MRI Devices Corp., Waukesha, USA), was used for imaging studies in patients with brainstem cavernomas. Each imaging session included a DTI scan and an anatomical imaging study, including a gadolinium-enhanced scan for intraoperative navigation. The field of view for all scans was defined as 200×200 mm^2.

DTI data acquisition

For the DTI series, a whole brain diffusion-weighted single-shot spin-echo EPI sequence was applied with the following parameters: in-plane matrix=96×96, reconstructed to 128×128, 60 contiguous slices, slice thickness=2.1 mm, TE=50 ms, number of signal averages=2, 60 % partial *k*-space acquisition. Diffusion weighting with a maximal *b*-factor of 1,000 s/mm^2 was carried out along 15 icosahedral directions complemented by one scan with $b=0$.

DTI data post-processing

Fiber tracking was performed using Philipps workstation (Achieva, Best, the Netherlands) with an according reconstruction software program (RELEASE) of the above mentioned MR system.

Table 1 Clinical and surgical characteristics of patients

No.	Age	Sex	Location	Size (mm)	Volume (mm3)	Approach	Discharge at day	FU months	Motor grade						Sensory deficit						KPS			Patzold		
									0 MG L	0 MG R	1 MG L	1 MG R	2 MG L	2 MG R	0 SD L	0 SD R	1 SD L	1 SD R	2 SD L	2 SD R	0	1	2	0	1	2
1	25	F	midbrain, pons	4.3×2.8×2.4	28.9	Retromastoidal	14	3	3	5	4	5	5	5	2	3	3	3	3	3	70	70	80	15	6	3
2	47	F	pons	3.0×2.7×2.6	21.1	Suboccipital	45	3	4	5	4	5	4	5	2	3	2	3	2	3	70	50	70	17	17	11
3	45	F	pons	3.1×2.6×2.5	20.2	Suboccipital	14	6	2	5	3	5	3	5	1	3	1	3	2	3	40	60	70	31	10	7
4	29	F	cerebellar peduncle	3.0×2.8×2.3	19.3	Suboccipital	18	6	4	5	5	5	5	5	2	3	3	3	3	3	50	60	70	16	4	3
5	39	F	pons	2.3×2.8×2.7	17.4	Retromastoidal	16	6	5	5	5	5	5	5	2	3	2	3	2	3	70	70	80	7	6	6
6	32	F	pons	2.2×2.3×3.1	15.7	Subtemporal	14	3	4	5	4	5	5	5	3	3	3	3	3	3	70	80	90	18	6	2
7	44	F	pons	2.7×2.9×1.9	14.9	Suboccipital	9	3	5	4	5	5	5	5	3	2	3	3	3	3	70	80	90	21	7	2
8	57	F	midbrain	2.6×1.8.×3.0	14.0	Medial frontobasal	19	6	4	2	4	2	4	3	2	2	2	2	2	2	20	50	50	42	31	23
9	6	M	pons	2.6×2.0×2.5	13.0	Retromastoidal	14	3	4	5	4	5	5	5	3	3	3	3	3	3	70	70	80	8	7	6
10	50	M	pons	2.2×2.1×2.0	9.2	Suboccipital	15	3	4	5	4	5	4	5	2	3	2	3	2	3	60	60	60	23	19	18
11	30	M	pons	2.2×2.1×2.0	9.2	Retromastoidal	24	3	5	5	5	5	5	5	2	3	3	3	3	3	70	70	90	4	1	1
12	38	M	crus cerebri	2.2×1.8×1.7	6.1	Subtemporal	11	3	4	5	5	5	5	5	3	3	3	3	3	3	80	80	80	6	3	2
13	26	F	pons	1.6×1.7×1.9	5.2	Suboccipital	10	3	5	5	5	5	5	5	3	3	3	3	3	3	70	70	70	6	5	4
14	14	F	pons	1.7×1.7×1.7	4.9	Retromastoidal	11	3	5	5	5	5	5	5	3	3	3	3	3	3	80	80	90	5	2	2
15	22	F	pons	2.1×1.2×1.5	3.8	Suboccipital	24	4	4	5	5	5	5	5	2	3	2	3	2	3	70	60	70	13	9	8
16	47	F	pons	1.6×1.5×1.5	3.6	Retromastoidal	17	3	5	5	5	5	5	5	2	3	2	3	2	3	70	70	70	9	4	4
17	34	F	pons	1.4×1.7×1.5	3.6	Supracerebellar	17	3	5	4	5	4	5	4	3	2	3	2	3	2	60	70	70	12	10	7
18	52	F	midbrain, pons	1.6×1.5×1.1	2.6	Suboccipital	19	3	5	5	5	5	5	5	3	2	3	2	3	2	70	80	90	9	4	3
19	23	M	pons	1.5×0.8×2.0	2.4	Suboccipital	16	6	5	5	5	5	5	5	3	3	3	3	3	3	80	80	90	3	2	1
20	51	F	pons		1.2	Supracerebellar	11	6	5	4	5	5	5	5	3	2	3	3	3	3	70	80	90	12	7	3

Table 1 (continued)

No.	Age	Sex	Location	Size (mm)	Volume (mm3)	Approach	Discharge at day	FU months	Motor grade						Sensory deficit						KPS			Patzold		
									0 MG L	0 MG R	1 MG L	1 MG R	2 MG L	2 MG R	0 SD L	0 SD R	1 SD L	1 SD R	2 SD L	2 SD R	0	1	2	0	1	2
				1.1×0.9×1.2																						
21	63	F	medulla oblongata	1.0×1.0×1.1	1.1	Suboccipital	21	3	5	5	5	5	5	5	3	3	3	3	3	3	70	80	90	6	5	4
22	45	F	pons	1.4×0.8×0.8	0.9	Retromastoidal	12	3	5	5	5	5	5	5	3	3	2	3	3	3	80	80	90	2	2	1
23	19	F	pons	1.0×0.8×0.8	0.6	Retromastoidal	8	5	5	4	5	4	5	4	3	3	3	2	3	2	70	70	80	10	8	7
Min	6				0.6		8	3													20	50	50	2	1	1
Median	38				6.1		15	3													70	70	80	10	6	4
Max	63				28.9		45	6													80	80	90	42	31	23

0 preoperative, *1* postoperative, *2* follow-up, *L* left, *R* right, *MG* motor grade, *SD* sensory deficit, *KPS* Karnofsky Performance Scale

White matter fiber tracking

White matter fiber tracking was performed by a continuous tracking algorithm with a fractional anisotropy of 0.42 and an angle of 60. Multiple ROIs were applied according to the anatomical landmarks used by Kamali et al. [16] for the medial lemniscus and to the landmarks used by Stieltjes [33] and Wakana [36] for the corticospinal tract. Image quality was optimized according to visualization values, and anatomic accuracy was based on atlases of diffusion tensor imaging anatomy. The reconstructed fibers were rated on each slice to provide similarity to the above-mentioned anatomic landmarks and to the reference atlas images. Three ROIs were applied for each pathway. A tracking operation was performed by selecting only the fibers that passed through the placed ROIs in the DTI-colored map. After reconstruction, some crossing pontine or midline fibers were removed by an additional operation (NOT).

Corticospinal tract

The fiber tracking of the corticospinal tract was obtained by placing three different ROIs along the pathway. The first ROI was located on the lowest level of the upper medulla in the area of the corticospinal tract above the decussation of the pyramids. The second ROI was placed on the posterior limb of the intern capsule, and the third ROI was placed on the highest level of the primary motor cortex. For the three different ROIs, tracking operations were selected. Only fibers passing through the located ROIs in the above mentioned areas were selected for fiber tracking.

Exemplary quantitative analyses of corticospinal tracts

For quantificational purposes, alterations of the corticospinal tracts were quantified in our first illustrative case. Three different ROIs, on different levels (a. upper part of the medulla, b. lesion, c. internal capsular) with a voxel size of >5 were drawn on each side and compared to the pre- and postoperative changes. Fractional anisotropy (FA) maps were generated on axial planes in color-coded maps to quantify pre- and postoperative alterations.

Medial lemniscus

Conscious proprioceptive and tactile information are transmitted in the medial lemniscus as a principal ascending pathway, originating in the dorsal column nuclei in the caudal medulla. The medial lemniscus decussates in the lower medulla on the level of the sensory decussation and hits the VPL nucleus of the thalamus. Three ROIs were applied to obtain the medial lemniscus pathway. The first ROI was located over the lowest

visible level of the red nuclei. The second ROI was applied over the pontine tegmentum at the side of the first placed ROI, and the third was applied over the area of the VPL of the thalamus. Beyond the thalamus, the fibers continue toward the somatosensory cortex. A tracking operation was performed and some fibers passing through the thalamus or crossing the pontine area were removed with additional deleting operations.

Surgical procedure

All patients underwent microsurgical resection of a symptomatic BSC. Surgical approaches depended on the size and location of the lesion and included the following approaches: 10 suboccipital, 8 retromastoidal, 2 supracerebellar, 2 subtemporal, and 1 medial frontobasal. The surgical route was determined according to the side and size of the lesion, as well as its spatial relationships to critical structures, such as the corticospinal and sensory tracts. Multimodality intraoperative monitoring was used to support the surgeon and included motor-evoked potentials (MEP) [30], somatosensory-evoked potentials (SEP), acoustic-evoked potentials (AEP), neuronavigation, and mapping of the romboid fossa [6].

Image interpretation

Corticospinal and sensory tracts were visualized on the basis of DTI. The relationship between the visible fibers and the lesion with its surrounding edema was analyzed, focusing on displacement, fiber bundle thickness, and the disruption of fibers. We analyzed the medial lemniscus (LM) and the corticospinal tract (CS) for the left and the right sides. Visibility was scored as "good" (++, 2 points: correct fiber bundle visualization), "low" (+, 1 point: partial fiber bundle visualization in the normal anatomic location), and "none" (−, 0 points: non-visibility of fiber bundles at all). For each patient, the preoperative scores were added to obtain a degree of visibility. Corresponding preoperative white matter tracts (in 21 cases) were compared with respect to the postoperative expansion of bundle thickness and to their degree of visibility. Neurological deficits of each patient assessed on admission were compared with the size and location of the lesion observed on T1- and T2-weighted MRI-images, and the appearance of the fiber tracts was visualized by DTI. Postoperative neurological changes were analyzed in relation to the corresponding anatomical structures that were visible on the imaging.

Results

Conventional MR imaging evaluation

BSC volume was calculated based on cross-sections of the lesions on axial, coronal, and sagittal MR images, with a range of 0.6 up to 28.9 mm^3 (median 9.7 mm^3) (Table 1).

Neurological evaluation and follow-up

Different combinations of neurological deficits were assessed on admission: motor deficits (n=12) and sensory deficits (n=14). Patients were discharged between 8 to 45 days, with a median of 15 days, and the first follow-up was between 3 and 6 months after surgery, with a median of 3 months (Table 1).

Out of the 23 patients included in this study, 13 (57 %) presented with motor deficits before surgery. Nine of these 13 (69 %) showed an improvement upon follow-up. The other 4 (31 %) maintained their level of performance after surgery and follow-up. Postoperatively, no motor deficits were induced (Table 1).

Fourteen of our 23 patients (60 %) showed sensory deficits before surgery. Of those fourteen, six (42 %) showed improvement of their sensory deficits on follow-up, another seven (50 %) remained unchanged, and one patient (7 %) showed additional sensory deficits on follow-up (Table 1).

Effect of surgery on neurosurgical outcome

Karnofsky performance status scale improvement

For all patients (N=23), the KPS ratings for the preoperative period, upon discharge and upon follow-up, are illustrated in Fig. 1. The median KPS was 70 % preoperatively and 80 % at the last follow-up. Upon discharge, the KPS improved in 9 out of 23 patients (39 %), remained equal in 12 (52 %), and deteriorated in 2 patients. Upon the last follow-up, the KPS improved in 17 out of 23 patients (74 %), remained equal in 6 (26 %), and deteriorated in 0 (0 %). KPS improvement is statistically significant, with p=0.0002 (Wilcoxon sign rank test).

Patzold Rating improvement

Preoperatively, the median PR was 10.0 and it was 4.0 on follow-up. Upon discharge, the PR improved in 21 out of 23 patients (91 %), 2 (9 %) remained equal and the neurological status was worse after surgical treatment in 0 patients. On last follow-up, the PR improved in 19 out of 23 patients (83 %), in 4 patients (17 %) it remained equal, and it deteriorated in 0 patients (0 %). The improvement in the Patzold Rating was statistically significant, with p=0.0002 (Wilcoxon sign rank test).

Preoperative visualization of corticospinal and sensory tracts

The right corticospinal tract could be visualized in 17 cases (81 %) with *good visibility*; 2 cases (10 %) showed a *low visibility*, and in 2 cases (10 %), no *visibility* was possible. The left corticospinal tract was visualized with *good visibility* in 15 cases (71 %), 4 cases (20 %) showed *low visibility,* and in 2 cases (10 %), *no visibility* was possible. In total (right and left), 90 % of the CSTs were visualized. The sensory tract on the right side was preoperatively visualized in 11 cases (52 %) with *good visibility*; three cases (14 %) showed *low visibility,* and 7 cases (33 %) showed *no visibility*. On the left side, 15 cases (71 %) showed *good visibility*, 2 cases (10 %) showed *low visibility*, and 4 cases (19 %) showed *no visibility*. In total (right and left), 74 % of the STs were visualized.

Postoperative visualization of corticospinal and sensory tracts

In the postoperative DTI sequences, the right corticospinal tract could be displayed 12 times (80 %) with *good visibility*, in 2 cases (13 %) showed *low visibility*, and one case (6 %) showed *no visibility*. The left corticospinal tract was displayed 12 times (80 %) with *good visibility* and 3 times (20 %) with *low visibility*. In total (right and left), the CSTs were visualized in 97 % of the cases.

In terms of postoperative sensory tracts, the right sensory tract was visualized in *good visibility* in 8 cases (53 %). In 3 cases (20 %), *low visibility* was shown, and in 4 cases (26 %), *no visibility* was displayed. The left sensory tract was visualized in 8 postoperative cases (53 %) with *good visibility*, five cases (33 %) with *low visibility*, and 2 cases (13 %) with *no visibility*. In total (right and left), the ST were visualized in 80 % of the cases.

Comparison of pre- and postoperative visualization of corticospinal and sensory tracts

In the 13 cases in which preoperative and postoperative visualization of corticospinal and sensory tracts was carried out, we observed a reduction in corticospinal fibers in two cases (case 3 and case 18). In one case (case 23), the sensory tracts showed a significant reduction in thickness on the left side, and they were no longer visible on the right side.

Illustrative case I

This patient (case no. 1, Fig. 1) is a 25-year-old female with a cavernous malformation (4.3×2.8×2.4 mm; 28.9 mm^3) at the junction of pons and midbrain. The mayor preoperative DTI finding displayed thinning of the right CST. Preoperatively, the patient presented with a hemiparesis on the left. The patient was operated via a retromastoidal approach. Postoperatively, our imaging data showed that the lesion was removed and the right CST appeared thicker. This was reflected clinically by improvement of the hemiparesis.

Quantitative analyses of corticospinal tracts with DTI

For exemplary purposes, we quantified the pre- and postoperative alterations of the corticospinal tracts with DTI (FA maps) in our first illustrative case. Preoperatively, we displayed higher FA values on lesions side in comparison to the postoperative situation, indicating early reorganization of corticospinal tracts after cavernoma removal. Preoperative FA measurement of the corticospinal tracts superiorly (internal capsule) and inferiorly (upper part of medulla) to the lesion showed lower FA values in comparison to the postoperative situation indicating no early reorganization after lesion removal.

Illustrative case II

This patient (case no. 7, Fig. 2) is a 44-year-old female with a cavernous malformation (2.7×2.9×1.9 mm; 14.9 mm^3) in the central pons. On admission, she presented with a right-sided hemiparesis (M4) and a moderate right-sided sensory deficit. Preoperatively, she showed bilateral deficits in cranial nerves III, IV, and VI. The mayor DTI findings displayed a distortion and a predominantly left-sided thinning and interruption of the corticospinal fibers adjacent to the lesion, correlating well with its space-occupying effect and the right-sided hemiparesis. Furthermore, the sensory tracts were displaced from their normal anatomic position, corresponding well with the preoperative sensory neurological status. The patient underwent surgery via a left suboccipital approach. The entry point into the brainstem was at the ponto-medullary sulcus. Postoperatively, our imaging data showed that the lesion had been completely removed and the corticospinal and sensory tracts had returned back into their regular anatomical location. The patient showed an improvement in her hemiparesis and sensory deficits upon discharge (day 9). At the 3-month follow-up examination, normal motor function and significant improvements in her ocular movement were observed.

Illustrative case III

Figure 3 illustrates a case of a 38-year-old male (case no. 12) with a cavernous malformation (2.3×1.8×1.7 mm; 7.1 mm^3) in his right crus cerebri. Six weeks preoperatively, the patient developed a gradually increasing left-sided hemiparesis that also involved the

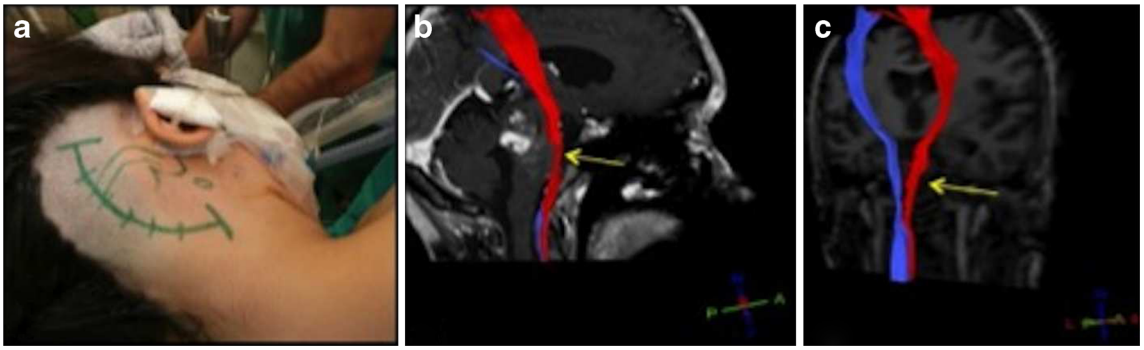

Fig. 1 Illustrative case I. The planned skin incision for the retromastoidal approach and patient position can be seen in **a**. The right corticospinal tract (**b**, *red*) showed thinning (*yellow arrow*) due to the space occupying effect of the cavernous malformation. Postoperatively, the lesion was removed completely and the right CST (**c**) showed thickening (*yellow arrow*) on lesion side

facial nerve. Four weeks preoperatively, a partial facial hypoesthesia occurred. In addition to preoperative visualization of the corticospinal and sensory tracts on the radiological viewing console, we processed both tracts on the Dextroscope (see Video, Supplemental Video, which demonstrates the second illustrative case). On this surgical planning system, the CT and MRI series can be fused, segmented, and displayed in a stereoscopic environment. DTI-derived white matter tracts can be computed and displayed in a spatial relationship to the cavernoma, the brainstem silhouette, and the skull base. In this case, the corticospinal tract ran lateral and anterior to the lesions, whereas the sensory tracts ran lateral and posterior to the lesions (Fig. 5b). A right subtemporal approach was simulated, and the entry point to the brainstem could be precisely determined between the corticospinal and sensory tracts (vertical dotted line). This spot of entry into the lateral side of the brainstem was marked on the MRI that was used for intraoperative navigation. A 3-mm vertical blunt dissection was carried out, and the cavernoma could be totally removed (Fig. 5c, d). During the first three postoperative days, the hemiparesis was slightly worse compared to the preoperative level; however, during the course of the following weeks and upon discharge, the situation improved markedly. At the 3-month follow-up examination, the patients' hemiparesis had subsided.

Illustrative case IV

Figure 4 illustrates case no. 15 of our study population. This patient was a 22-year-old female with a cavernous malformation in the right part of the pons. Preoperatively, the patient presented with a slight hemiparesis on the left. Postoperatively, our DTI imaging displayed intact course of the CSTs. The hemiparesis on the left subsided postoperatively.

Illustrative case V

Figure 5 illustrates case no. 6 of our series.

This patient was a 32-years-old female with a cavernous malformation in the pons. Preoperatively she presented with a slight hemiparesis on the left.

This patient was operated via a right temporal approach. The cavernous malformation was located in the right part of the pons, and the preoperative DTI finding displayed splitting of the right CST. The CST was deviated anterior and posterior. In the postoperative DTI reconstruction of the right CST, interruption is still visible. The left CST and both sensory tracts went back into the normal anatomical formation. On discharge, the slight hemiparesis was still present, but resolved during the follow-up.

Discussion

The aim of this study was to investigate the feasibility of DTI-based fiber tracking in patients with brainstem cavernomas, assessing the association between the pre- and postoperative appearance of the fiber tracts and clinical outcome.

Generating accurate fiber tracts is especially difficult in the area of the brainstem in which a variety of tracts and nuclei are in close proximity to each other. Preserving the integrity of fiber tracts within the brainstem is one of the limiting factors of successful brainstem surgery, and one may argue that the concept of maximum tumor resection [1] is not applicable in this region. Lesniak et al. showed that even careful resection of lesions in the brainstem still involves serious risks [21]. Imaging modalities, such as standard MRI, CT, and positron emission tomography (PET), have been used to determine the spatial location and extent of lesions in the brainstem. Unfortunately, they provide no additional information about eloquent fiber structures. This calls for a technology that supports the surgeon with reliable fiber tract visualization in order to preserve their integrity, rather than being forced to balance the

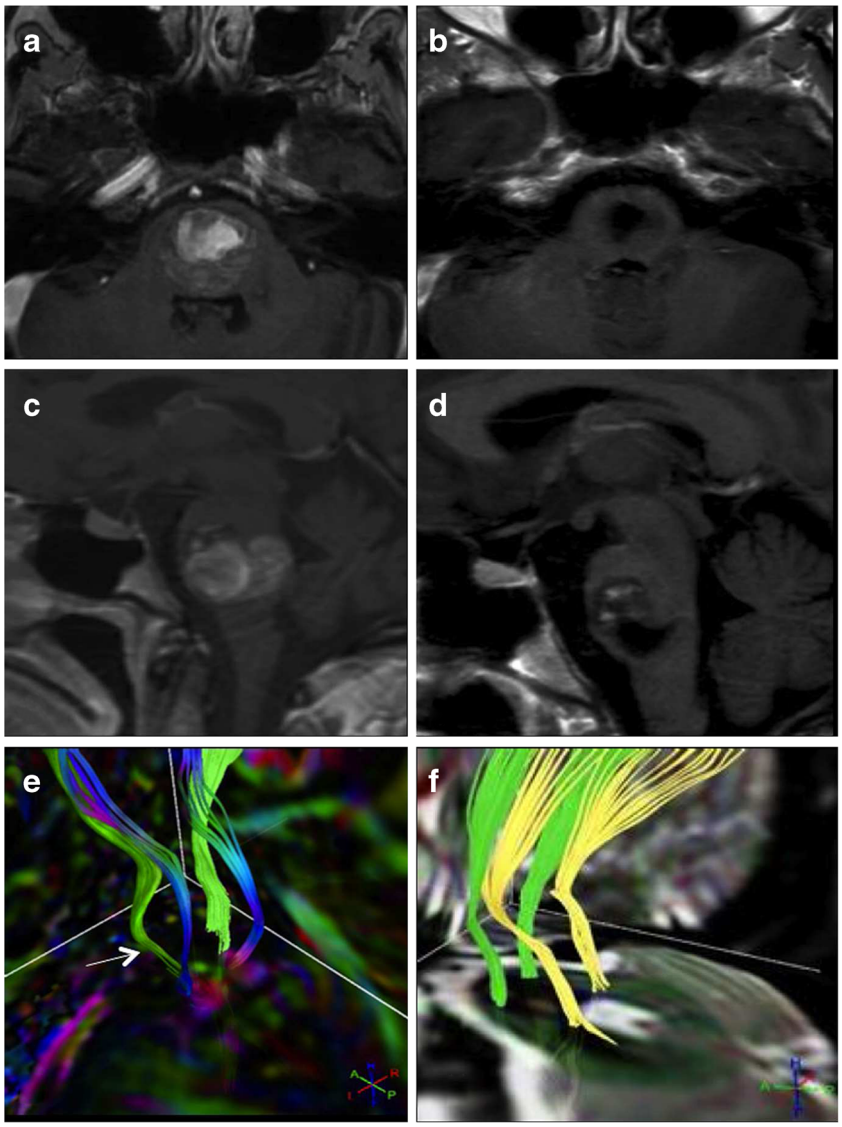

Fig. 2 Illustrative case II. Preoperative T1, GD-enhanced axial (**a**), sagittal (**c**), and DTI tractography (**e**). On DTI reconstruction (**e**), the space-occupying effect of the lesion with distortion and thinning (*white arrow*) of the corticospinal fibers (*green*) and sensory tracts (*blue*) are visible. Postoperative T1+GD axial (**b**), sagittal (**d**), and postoperative DTI (**f**). The structural displacement caused by the mass effect has been significantly reduced after resection. The corticospinal fibers (*green*) and sensory tracts (*yellow*) moved back to their regular anatomic positions

aim of total resection and the fear of neurological deficits. Advantages in DTI fiber-tracking technology have provided the neurosurgeon with a new tool to assess fiber tracts before and after surgical intervention. In other words, this could help to secure the integrity of fibers and at the same time remove as much of the lesion as necessary. Several studies have reported using DTI to map the effects of lesions in the white matter anatomy [10, 15, 20, 23, 26, 28, 39]. Nimsky et al. previously reported on DTI tractography in patients with brainstem lesions and illustrated its great value for brainstem surgery in terms of risk stratification, prognosis, and treatment strategies [9]. Furthermore, this group was able to implement DTI into a standard neuronavigation system to intraoperatively visualize fiber tracts [25]. We did not include our fiber tracts in our neuronavigation system in this study, but nevertheless, we found that DTI tractography provides the surgeon with valuable informations to evaluate and plan the surgical intervention. This was clearly demonstrated in our illustrative cases. In our first illustrative case (Fig. 1), the right CST showed preoperative thinning and displacement. Postoperatively, after lesion removal, the right CST was displayed in the regular anatomical position. In Illustrative case II (Fig. 2), the major preoperative DTI findings displayed a distortion and predominantly left-sided thinning of the corticospinal fibers adjacent to the lesion, correlating well with its space-occupying effect. Additionally, the sensory tracts were moved out of their correct anatomical positions, and we noticed that the neurology corresponded well with the distortion of the tracts. We decided to operate on the patient via a left suboccipital approach. The entry point into the brainstem was at the ponto-medullary sulcus. Looking at the MRI data postoperatively, we found that the lesion had been removed and the fiber tracts had been preserved during surgery. Corticospinal tracts and sensory tracts had moved back to their normal anatomical position and organization. On the 3-month follow-up clinical examination, we observed a full regression of hemiparesis and a significant improvement in eye movement.

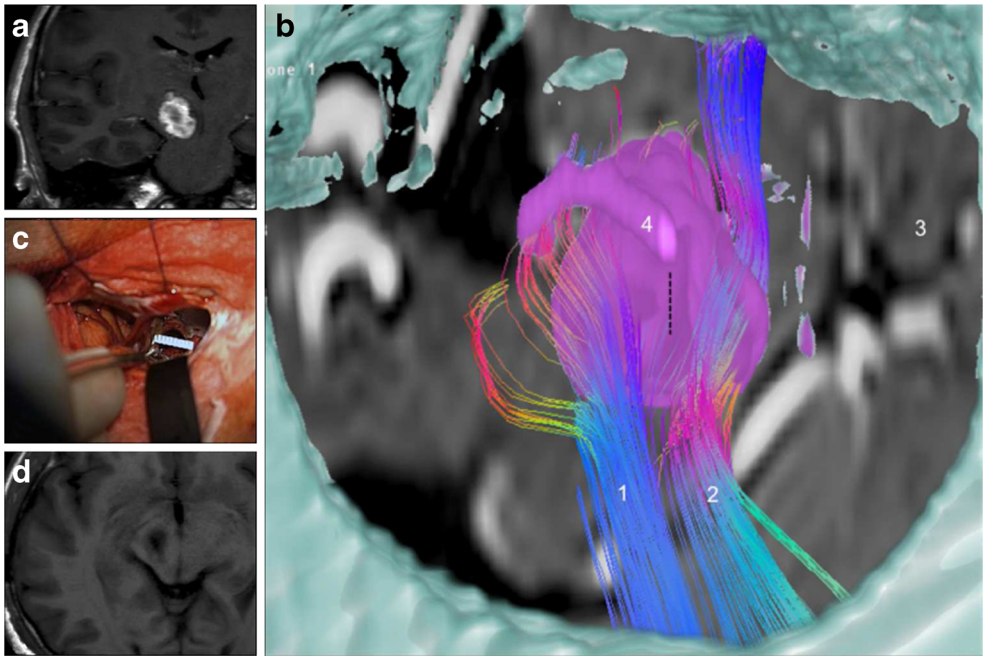

Fig. 3 Illustrative case III. In **a**, the large, hemorrhagic cavernous malformation is observed in the right crus cerebri via T1-W coronal MR imaging. **b** Shows the preoperative visualization in the Dextroscope, simulating a right subtemporal approach. The cavernoma (*pink*, segmented from MRI) is surrounded anteriorly by the corticospinal tract (*1*) and posteriorly by the sensory fibers of the medial lemniscus (*2*). A moveable sagittal MRI plane (*3*) shows the relationship to the brainstem. The skull and middle cranial fossa are fused with the MRI data and a middle fossa craniotomy was simulated. The dotted vertical line above the cavernoma indicates the entry point into the brainstem between the two fiber bundles. The PCA (*4*) was shown to run within the surgical corridor; intraoperatively, it was mobilized and moved upwards. **c** Shows the intraoperative view; the ruler marking the opening of the brainstem after the cavernoma had been removed. Total removal of the lesion without damage of the brainstem is demonstrated on postoperative MRI in the axial in D

Just a moderate palsy of cranial nerve VI remained. Exemplarily, we quantified alterations of pre- and postoperative changes in the corticospinal fibers in our first illustrative case. We concluded possible appearance of early reorganization in the corticospinal tracts after cavernoma removal corresponding well with the postoperative tracking of the corticospinal fibers. Despite the fact that measurements superiorly and inferiorly to the lesion did not show improvements in alterations. In the future, one of our groups around Kollias et. al will show the potential of DTI quantification in brainstem surgery in 3 T-MRI.

In our third illustrative case, (see Video, Supplemental Video, which demonstrates the second illustrative case), the corticospinal as well as the sensory tracts were visualized to be spread out lateral to the lesion (Fig. 3b). In addition to the visualization of the fiber tracts on the radiological viewing console, we used the Dextroscope for surgical planning for this case as well as for three other cases. The Dextroscope contains its own tractography module, which can be used to generate fiber tracts based on the DICOM DTI series. When placing the ROIs in the Dextroscope in a similar fashion as on

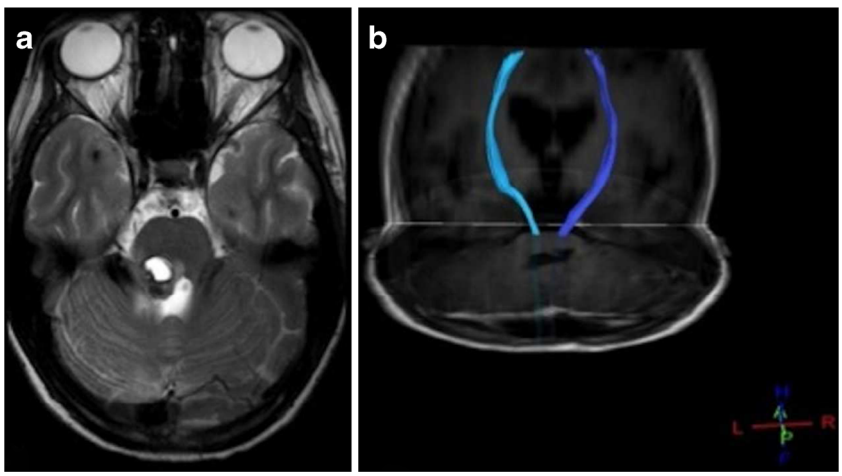

Fig. 4 Illustrative case IV. Preoperative T2-W axial MR image (**a**) with space occupying BSC in the pons. The postoperative T1-W axial/coronal MR image (**b**) with reconstructed CSTs confirmed the intact postoperative course of both CSTs

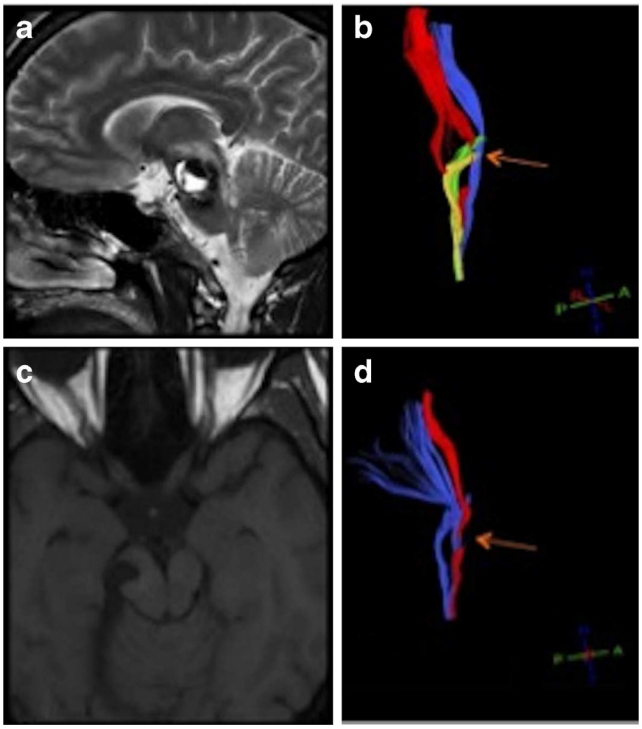

Fig. 5 Illustrative case V. Preoperative T2-W sagittal MR image (**a**) with cavernous malformation in the right part of the pons. The right corticospinal tract (*red*) is deviated and interrupted (*orange arrow*) due to the BSC (**b**). The sensory tracts (*yellow and green*) showed no signs of interruption. The left CST (*blue*) is slightly deviated with no signs of interruption. Postoperatively (**c**) the lesion was removed completely. In the postoperative reconstruction (**d**) of the right CST, the interruption (*orange arrow*) is still visible which was reflected clinically as well

the radiological console, we found the position and the appearance of the tracts to be similar. The Dextroscope's additional advantage is the fact that the fiber tracts can be displayed in direct relationship to other, three-dimensionally segmented objects: the lesion, the brainstem surface, the skull base (segmented from CT), and the tentorium. Simulating a middle fossa craniotomy and the surgical viewpoint along this trajectory toward the lesion, we concluded that a right subtemporal approach would be most suitable. The opening of the brainstem was determined to be between the anteriorly located corticospinal tract and the posteriorly located sensory tract (Fig. 3b). The operation was carried out as simulated, and gross total cavernoma removal was achieved (Fig. 3c, d).

In all cases of this study, the tractography information allowed for the accurate planning of the surgical path and the gross volume reduction of the cavernomas. Although the fiber tracts were not displayed in the navigation system, knowing the exact position of the fibers on preoperative MR imaging enabled the exact identification of the most suitable entry point into the brainstem. We would then intraoperatively identify this entry zone with the help of MRI-based navigation, keeping in mind the position of the fiber tracts to be avoided.

The postoperative neurological improvement could be clearly related to the postoperative repositioning of fiber tracts and alteration in thickness in most of our cases. In illustrative case IV (Fig. 4), the postoperatively reconstructed CSTs on both sides confirmed fiber tract integrity, which was reflected clinically by resolving of the hemiparesis. In illustrative case V (Fig. 5), the postoperative reconstruction of the right CST showed interruption. This was reflected since on discharge the hemiparesis was still present, but resolved completely on follow-up.

In approximately 75 % of the cases (KPS) and over 80 % of the cases (PR), the patients showed a long-term improvement at follow-up. In those cases, fiber repositioning and thickening was observed. These patients tended to have a better neurological recovery at the long-term follow-up. All postoperative cases showed that the corticospinal tracts could be preserved; only two cases (case 3 and case 18) showed reduction in the corticospinal tract visibility, which was not observed clinically. Only one postoperative case (case 23) showed a loss and reduction of the sensory tracts after surgery, which was reflected clinically by a mild hemisensory deficit.

DTI technology is rapidly emerging; however, there are still restrictions to be considered when integrating it in routine neurosurgical planning. Tropine et al. have demonstrated that in defining the cause of altered DTI signals in the presence of supratentorial gliomas, the difference between tumor infiltration and vasogenic edema might not be clearly distinguished. [34] Furthermore, Price et al. showed that extra effort is needed to find the relationship between peritumoral DTI sequences and tumor characteristics[28], again stating that the currently available DTI technology can hardly distinguish between tumor infiltration and edema.

One main limitation of our retrospective study was the small number of patients. Despite all that, to our knowledge, this is the largest series of brainstem cavernoma patients that have been evaluated with respect to the feasibility of DT imaging.

In the future, more refined DTI acquisition and post-processing technology may enable the improved differentiation and more accurate display of tracts within the brainstem, including fine tracts related to brainstem nuclei and those tracts interconnecting them. Especially combined with intraoperative MRI, these developments will lead to an even more accurate determination of safe entry zones into the brainstem and dissection routes toward target lesions.

Conclusions

Our study demonstrated that DTI allows for accurate and detailed white matter tract visualization, even in cases of lesions in the brainstem. Visualizing the tracts adjacent to the lesion adds to our understanding of the distorted intrinsic brainstem anatomy and enhances the perception for planning the surgical approach.

Acknowledgments We thank Peter Roth from the Department of Neurosurgery at the University Hospital Zurich for providing expert support for illustrations in our illustrative cases.

Disclosure The authors have no personal financial or institutional interest in any of the materials or devices described in this article.

Conflict of interests There are no competing interests.

References

1. Ammirati M, Vick N, Liao YL et al (1987) Effect of the extent of surgical resection on survival and quality of life in patients with supratentorial glioblastomas and anaplastic astrocytomas. Neurosurgery 21:201–206
2. Arfanakis K, Gui M, Lazar M (2006) Optimization of white matter tractography for pre-surgical planning and image-guided surgery. Oncol Rep 15:1061–1064
3. Barboriak DP (2003) Imaging of brain tumors with diffusion-weighted and diffusion tensor MR imaging. Magn Reson Imaging Clin N Am 11:379–401
4. Bello L, Gambini A, Castellano A et al (2008) Motor and language DTI Fiber Tracking combined with intraoperative subcortical mapping for surgical removal of gliomas. Neuroimage 39:369–382
5. Bertalanffy H, Benes L, Miyazawa T et al (2002) Cerebral cavernomas in the adult. Review of the literature and analysis of 72 surgically treated patients. Neurosurg Rev 25:1–53, discussion 54–55
6. Bertalanffy H, Tissira N, Krayenbuhl N et al. Inter- and intrapatient variability of facial nerve response areas in the floor of the fourth ventricle. Neurosurgery 68:23–31; discussion 31
7. Bozinov O, Hatano T, Sarnthein J et al. Current clinical management of brainstem cavernomas. Swiss Med Wkly 140:w13120
8. Cao Z, Lv J, Wei X et al. Appliance of preoperative diffusion tensor imaging and fiber tractography in patients with brainstem lesions. Neurol India 58:886–890
9. Chen X, Weigel D, Ganslandt O et al (2007) Diffusion tensor imaging and white matter tractography in patients with brainstem lesions. Acta Neurochir (Wien) 149:1117–1131, discussion 1131
10. Clark CA, Barrick TR, Murphy MM et al (2003) White matter fiber tracking in patients with space-occupying lesions of the brain: a new technique for neurosurgical planning? Neuroimage 20:1601–1608
11. Coenen VA, Krings T, Mayfrank L et al (2001) Three-dimensional visualization of the pyramidal tract in a neuronavigation system during brain tumor surgery: first experiences and technical note. Neurosurgery 49:86–92, discussion 92–83
12. Ferroli P, Sinisi M, Franzini A et al (2005) Brainstem cavernomas: long-term results of microsurgical resection in 52 patients. Neurosurgery 56:1203–1212, discussion 1212–1204
13. H. M (2000) Skalen und Scores in der Neurologie. Thieme Stuttgart, Baden-Württemberg
14. Hammerstad JN (2003) Strength and reflexes. In: Goetz CG (ed) Textbook of clinical neurology. Elsevier Science, Philadelphia, pp 225–265
15. Holodny AI, Schwartz TH, Ollenschleger M et al (2001) Tumor involvement of the corticospinal tract: diffusion magnetic resonance tractography with intraoperative correlation. J Neurosurg 95:1082
16. Kamali A, Kramer LA, Butler IJ et al (2009) Diffusion tensor tractography of the somatosensory system in the human brainstem: initial findings using high isotropic spatial resolution at 3.0 T. Eur Radiol 19:1480–1488
17. Kikuta K, Takagi Y, Nozaki K et al (2008) Introduction to tractography-guided navigation: using 3-tesla magnetic resonance tractography in surgery for cerebral arteriovenous malformations. Acta Neurochir 103:11–14
18. Kovanlikaya I, Firat Z, Kovanlikaya A et al. Assessment of the corticospinal tract alterations before and after resection of brainstem lesions using Diffusion Tensor Imaging (DTI) and tractography at 3 T. Eur J Radiol 77:383–391
19. Krishnan AP, Asher IM, Davis D et al (2008) Evidence that MR diffusion tensor imaging (tractography) predicts the natural history of regional progression in patients irradiated conformally for primary brain tumors. Int J Radiat Oncol Biol Phys 71:1553–1562
20. Lazar M, Weinstein DM, Tsuruda JS et al (2003) White matter tractography using diffusion tensor deflection. Hum Brain Mapp 18:306–321
21. Lesniak MS, Klem JM, Weingart J et al (2003) Surgical outcome following resection of contrast-enhanced pediatric brainstem gliomas. Pediatr Neurosurg 39:314–322
22. Mathiesen T, Edner G, Kihlstrom L (2003) Deep and brainstem cavernomas: a consecutive 8-year series. J Neurosurg 99:31–37
23. Mori S, Frederiksen K, van Zijl PC et al (2002) Brain white matter anatomy of tumor patients evaluated with diffusion tensor imaging. Ann Neurol 51:377–380
24. Naidich TP, Duvernoy HM, Delman BN et al. (2009) Duvernoy's Atlas of the Human Brain Stem and Cerebellum: High-Field MRI, Surface Anatomy, Internal Structure, Vascularization and 3 D Sectional Anatomy. Springer Wien New York
25. Nimsky C, Ganslandt O, Fahlbusch R (2006) Implementation of fiber tract navigation. Neurosurgery 58:ONS-292-303; discussion ONS-303-294
26. Nimsky C, Ganslandt O, Hastreiter P et al (2005) Preoperative and intraoperative diffusion tensor imaging-based fiber tracking in glioma surgery. Neurosurgery 56:130–137, discussion 138
27. Nimsky C, Grummich P, Sorensen AG et al (2005) Visualization of the pyramidal tract in glioma surgery by integrating diffusion tensor imaging in functional neuronavigation. Zentralbl Neurochir 66:133–141
28. Price SJ, Pena A, Burnet NG et al (2004) Tissue signature characterisation of diffusion tensor abnormalities in cerebral gliomas. Eur Radiol 14:1909–1917
29. Samii M, Eghbal R, Carvalho GA et al (2001) Surgical management of brainstem cavernomas. J Neurosurg 95:825–832
30. Sarnthein J, Bozinov O, Melone AG et al. Motor-evoked potentials (MEP) during brainstem surgery to preserve corticospinal function. Acta Neurochir (Wien) 153:1753–1759
31. Spena G, Nava A, Cassini F et al. Preoperative and intraoperative brain mapping for the resection of eloquent-area tumors. A prospective analysis of methodology, correlation, and usefulness based on clinical outcomes. Acta Neurochir (Wien) 152:1835–1846
32. Steinberg GK, Chang SD, Gewirtz RJ et al (2000) Microsurgical resection of brainstem, thalamic, and basal ganglia angiographically occult vascular malformations. Neurosurgery 46:260–270, discussion 270–261
33. Stieltjes B, Kaufmann WE, van Zijl PC et al (2001) Diffusion tensor imaging and axonal tracking in the human brainstem. Neuroimage 14:723–735
34. Tropine A, Vucurevic G, Delani P et al (2004) Contribution of diffusion tensor imaging to delineation of gliomas and glioblastomas. J Magn Reson Imaging 20:905–912
35. Ture U, Yasargil MG, Friedman AH et al (2000) Fiber dissection technique: lateral aspect of the brain. Neurosurgery 47:417–426, discussion 426–417
36. Wakana S, Jiang H, Nagae-Poetscher LM et al (2004) Fiber tract-based atlas of human white matter anatomy. Radiology 230:77–87
37. Wang CC, Liu A, Zhang JT et al (2003) Surgical management of brain-stem cavernous malformations: report of 137 cases. Surg Neurol 59:444–454, discussion 454
38. Witwer BP, Moftakhar R, Hasan KM et al (2002) Diffusion-tensor imaging of white matter tracts in patients with cerebral neoplasm. J Neurosurg 97:568–575
39. Yu CS, Li KC, Xuan Y et al (2005) Diffusion tensor tractography in patients with cerebral tumors: a helpful technique for neurosurgical planning and postoperative assessment. Eur J Radiol 56:197–204

Comments

Vini G. Khurana, Canberra, Australia

This is a beautifully written manuscript that reports a very thoughtfully and elegantly executed study of tractography in brainstem cavernous malformation surgery. The work represents a very helpful contribution to our understanding of how relatively high-risk surgery might be made more accurate and safe through a more "visible" and intuitive modality such as DTI compared with electrophysiology and neuronavigation alone. The five illustrative cases provide an elegant and almost tangible insight into the authors' exploration of this exciting frontier. I congratulate Doctor Ulrich and his colleagues on their inspirational work.